PHYSICAL REVIEW B VOLUME 43, NUMBER 2 15 JANUARY 1991-I

Coulombic and neutral trapping centers in silicon dioxide

D. A. Buchanan
IBM General Technology Division, East Fishkill Facility, Route 52, Hopewell Junction, New York 12533

M. V. Fischetti and D. J. DiMaria
IBM Research Division, Thomas J. Watson Research Center, P.O. Box 218, Yorktown Heights, New York 10598
(Received 11 July 1990)

Metal-oxide-semiconductor structures incorporating thermally grown silicon dioxide films were implanted with arsenic ions and then annealed at high temperatures. The subsequent trapping sites produced are amphoteric. Coulombic-attractive traps (for electrons) were produced with the avalanche injection of holes from the silicon substrate and the subsequent capture of some of these holes on the arsenic-related sites. During internal photoemission of electrons from a thin aluminum gate, the voltage shifts due to hole annihilation by electrons were recorded and the effective capture cross section was determined. This capture cross section was found to vary from $\sim 10^{-12}$ to 3×10^{-15} cm^2 for average electric fields ranging from 2×10^5 to 3×10^6 V/cm. An average field threshold ($\sim 1.2\times10^6$ V/cm) was found, below which the capture-cross-section–average-field dependence follows a power law with an exponent of approximately -1.5. Above the average field threshold, the power-law exponent was found to be approximately -3.0. Also, when the amphoteric arsenic-related sites are empty, they can form neutral trapping sites for electrons. For these trapping centers, it is found that the neutral capture cross section is relatively independent of the average electric field. For average fields ranging from 5×10^5 to 6×10^6 V/cm, the neutral cross section is found to be approximately constant at $(1\text{–}2)\times10^{-15}$ cm^2. For the Coulombic electron traps, classical and quantum-mechanical Monte Carlo simulations agree qualitatively with the experimental results. These simulations suggest that the heating of the electron-energy distribution and tunnel detrapping are the primary cause of the decrease in the effective capture cross section in the high-field regime. For the neutral traps in the low-field regime, the classical Monte Carlo simulation also agrees with the experimental results. However, for fields above the electron-heating threshold, the simulation predicts an increase in the capture cross section not found in the experimental data. We suggest that this discrepancy arises since the classical simulation does not account for tunnel detrapping, which would lower the effective cross section.

I. INTRODUCTION

In recent years, there has been a growing interest in the electronic properties of trapping centers found in silicon dioxide (SiO_2) used in metal-oxide-semiconductor (MOS) technologies. With the increasing demand for faster and more dense devices, both charged and neutral trapping centers have been found to be important in the role of degradation and breakdown mechanisms, especially in submicron metal-oxide-semiconductor field-effect transistors (MOSFET's). Even the so-called intrinsic (process-dependent) centers commonly found in SiO_2 today can be strongly affected by the large electric fields that are necessary as device dimensions decrease. And even though these centers may have very small capture cross sections,[1,2] significant threshold voltage shifts and even catastrophic breakdown can still result, since at high electric fields trap creation results.[1–12] Therefore it has become necessary to study these trapping centers with much better control than previously reported. Of particular interest, of course, is the field dependence of the capture cross section for both Coulombic and neutral electron-trapping centers, as both types of traps have been found to be prevalent in thermally grown SiO_2 films.

Measurements of many different types of traps in SiO_2 can be found in the literature. Unfortunately, researchers have had to rely on variations of processing conditions to produce trapping centers. As a result, the density, distribution, and position of the traps in such SiO_2 films are measurable, but generally uncontrollable. It is for these reasons that in our samples, trapping centers were produced with the implantation of arsenic ions (As^+) into the SiO_2 film. Therefore the density, position, and charge sign of the traps were controlled and could be verified experimentally. Also bulk trapping properties could be assessed, since with ion implantation (and subsequent pre- and post-metallization anneals), the traps could be positioned away from the Si/SiO_2 interface to reduce interface-state effects. It is known that trapping sites that are produced from As^+ implantation with high-temperature annealing treatments will trap both electrons and holes[13,14] with a large capture probability. Therefore by combining avalanche injection of holes from the silicon substrate (n type) and internal photoemission of electrons from the gate electrode, both neutral and Coulombic-attractive centers may be studied using the same sites.

Some preliminary results of this work have been pub-

 ©1991 The American Physical Society

lished previously.[15,16] However, this work is presented here in a complete manner, in full experimental and analytical detail.

II. SAMPLE FABRICATION

The substrates were n-type ⟨100⟩ silicon wafers with a resistivity of 0.1–0.2 Ω cm. After standard cleaning, a thermal oxide was grown in a nominally dry oxygen ambient at 1000 °C to a thickness of approximately 1240 Å (as determined by ellipsometry). The wafers were then given an As^+ implantation at room temperature. The ion concentration and energy for these samples were 5×10^{12} cm^{-2} and 60 keV, respectively. The wafers were then annealed in nitrogen at 800 °C for 30 min. Thin (∼120–150 Å) Al circular gate electrodes with an area of 5.2×10^{-3} cm^2 were deposited through a shadow mask from an rf-heated crucible at a pressure of 10^{-6} Torr to form MOS capacitors. The capacitors were given a postmetalization anneal (PMA) in forming gas (N_2/H_2) at 400 °C for 20 min to reduce the Si/SiO_2 interface-state density. Finally, the oxide from the back side of the wafer was etched to allow electrical contact. Control samples were similarly produced but contained no ion implantation.

III. MEASUREMENT PROCEDURES

Avalanche injection from the silicon substrate was used to inject holes into the SiO_2 film. In this technique the substrate is driven into deep depletion, where, under high electric fields, holes produced by impact ionization are injected into the SiO_2 film. Using an automated system, the amplitude of a 50-kHz sawtooth was continuously monitored in order to keep the average hole injection current constant. The ramp was periodically interrupted to measure the midgap voltage, which increased as some of the injected holes were trapped. The midgap voltage shift is defined as the shift in the high-frequency (1 MHz) capacitance-voltage (C-V) curve (when the Fermi level is at a silicon midgap position at the Si/SiO_2 interface), measured after charging, relative to the initial C-V curve. In this experiment, the total amount of initial charge (i.e., trapped holes) was varied by terminating the avalanche injection when the midgap voltage V_{mg} reached a certain desired value. The net midgap shift ΔV_{mg} was varied from ~ -2 to ~ -16 V.

After the sample had been charged to a predetermined state, electrons were injected from the Al gate using internal photoemission. A deuterium lamp (Oriel No. 6316) and an ultraviolet cutoff filter (Corning No. 9-54) were used to photoinject electrons from the Al gate into the SiO_2 film. The photocurrent was kept constant using a feedback system to control the applied bias. The midgap voltage shift, which now decreased as some of the injected electrons recombined at the trapped hole sites, was sensed during periodic interruptions of the injected current.

The use of midgap voltage to measure fixed oxide charge or oxide trapped charge has been reported previously.[17–20] This technique can eliminate the contribution of the charge in the interface states. Assuming, for simplicity, that the interface state are amphoteric and created by dangling silicon bonds or so-called P_b centers,[17,18] it has been shown that two electrons can be captured by each site as the Fermi level at the Si/SiO_2 interface is moved from the silicon valence band to the conduction band. The states above midgap are acceptorlike while those below midgap are donorlike, with equal numbers of each. (Each pair of donorlike and acceptorlike states corresponds to one P_b site.) Therefore when the Fermi level is at midgap, the interface is electrically neutral and the interface charge will not contribute to that sensed. It should be noted that, in general, not all interface states are P_b centers, nor need they be symmetric about midgap. However, for the capacitors used here, the density of interface states was low and symmetrical about midgap and we therefore assumed ΔV_{mg} to be an accurate measure of the net oxide trapped charge.

IV. ANALYSIS OF TRAPPING PROPERTIES

Using first-order kinetics, the rate equation for electron trapping can be written as[21]

$$\frac{dn_t}{dt}=k_c(N-n_t)-k_p n_t-k_t n_t \ , \tag{1a}$$

where

$$k_c=n_c\langle v_{\rm th}\rangle\sigma_c \ , \tag{1b}$$

$$k_p=\Phi_p\sigma_p \ , \tag{1c}$$

$$k_t=N_c v_{\rm th}\sigma_c \exp\left[\frac{-E_t}{k_B T}\right] . \tag{1d}$$

N is the density of traps, n_t is the density of filled traps, n_c is the density of conduction-band electrons, $\langle v_{\rm th}\rangle$ is the mean thermal velocity of an electron, σ_c is the microscopic capture cross section, Φ_p is the local photon flux, σ_p is the photoionization cross section, N_c is the effective density of states in the conduction band, and E_t is the trap depth measured from the conduction-band edge. The first term on the right-hand side of Eq. (1a) is the capture rate of thermal electrons from the conduction band. The last two terms are the detrapping rates by photon and phonon absorption, respectively.

The photoionization cross section for similar traps in SiO_2 has been found[13] to be more than an order of magnitude smaller than the trapping cross sections found in the present study. It is therefore assumed that the photodetrapping term in Eq. (1a) may be regarded as negligible.

The trap energy for electrons of the As-related traps is large (∼3.3 eV) relative to kT and therefore the probability of emission from the trap by multiphonon absorption is very small.[13] In this case, the final term is also negligible and Eq. (1a) may be approximated by

$$\frac{dn_t}{dt}\approx n_c v_{\rm th}\sigma_c(N-n_t) \ . \tag{2}$$

At high electric fields, the effective energy depth of the trapping center is reduced. In this regime, impact ioniza-

tion of a trapped electron, as well as tunnel detrapping (field ionization), may be significant. Initially, we have assumed that the above approximation is valid, at least for low electric fields, and that any detrapping mechanism will be absorbed in the field dependence of the capture cross section as discussed below.

The conduction-band current density is usually given by[21]

$$\frac{J(t)}{e}=n_c v_d \approx n_c v_{\text{th}} , \tag{3}$$

where e is the electron charge (-1.6×10^{-19} C) and v_d is the drift velocity of an electron. It has been shown[22] that for electric fields in the range $(0.2-0.8)\times10^6$ V/cm, the drift velocity is approximately equal to the thermal velocity of $\sim10^7$ cm/s. However, the electron-energy distribution is not in thermal equilibrium with the lattice for fields $\gtrsim1.5\times10^6$ V/cm, and significant electron heating occurs.[23–30] Under these conditions the above approximation is not valid, and $\sigma_c v_{\text{th}}$ [in Eqs. (1) and (2)] should be replaced by the average of the product of the microscopic cross section and carrier velocity over the actual *hot* electron-energy distribution. In any case, an effective cross section can be *defined* as $\sigma=\sigma_c v_{\text{th}}/v_d$, and we shall take this approach. With this substitution, Eq. (2) becomes

$$\frac{dn_t}{dt}=\frac{J}{e}\sigma(N-n_t) . \tag{4}$$

For the electron trapping case, n_t is the density of trapped electrons while $N-n_t$ is the density of Coulomb-attractive centers (i.e., trapped holes). It is assumed that the electrons are only trapped on the Coulombic sites. For most of the range of electric fields of interest, it has been found that this is valid. However, for higher electric fields ($\gtrsim3\times10^6$ V/cm) electron trapping on neutral sites (that is, on uncharged As-related centers) may no longer be neglected, since the capture cross section of the Coulombic centers approaches that of the neutral centers. This is discussed in more detail in Sec. VI.

Since the time evolution of trapped charge per unit area is the actual quantity that is measured experimentally, Eq. (4) must be integrated over the SiO_2 film thickness (d_{ox}) to give

$$\frac{dQ}{dt}=\frac{J}{e}\sigma(eN_t-Q) , \tag{5}$$

where

$$Q=e\int_0^{d_{\text{ox}}} n_t dx, \quad N_t=\int_0^{d_{\text{ox}}} N\,dx .$$

For any given time t, the total charge fluence is given by

$$N_{\text{inj}}(t)=\int_0^t \frac{J(t')}{e}dt' \quad \text{or} \quad \frac{dN_{\text{inj}}(t)}{dt}=\frac{J(t)}{e} . \tag{6}$$

Finally, substituting Eq. (6) into Eq. (5), the capture cross section is given by

$$\sigma=\frac{dQ}{dN_{\text{inj}}}\frac{1}{(eN_t-Q)} . \tag{7}$$

The midgap shift is related to the first moment of the oxide charge density per unit area by

$$\Delta V_{\text{mg}}=-\frac{\bar{x}Q}{\epsilon_{\text{ox}}} , \tag{8}$$

where $\bar{x}$ is the centroid of charge measured from the metal-SiO_2 interface and ϵ_{ox} is the static (or low-frequency) permittivity of the oxide. Using Eqs. (7) and (8), the capture cross section σ and density of traps N_t can be calculated when ΔV_{mg} is measured as a function of time. If the charge centroid ($\bar{x}$) is not known, σ may still be determined and an effective trap density may be calculated using

$$N_{t,\text{eff}}=\frac{\bar{x}}{d_{\text{ox}}}N_t . \tag{9}$$

For the capacitors used in this study, the position of the trapped charge centroid is determined by the implanted As^+ spatial distribution. Using secondary-ion mass spectroscopy[13,14] (SIMS) and the photo I-V measurements, the position of the charge centroid ($\bar{x}$) was verified experimentally.

During the injection of charge into the SiO_2 film, the external current (J_{ext}) was maintained at a constant value by adjusting the applied bias. In doing so, a displacement current component arises due to the changing applied bias. As the charge traverses the SiO_2 film, some of it is trapped, and contributes a component to the external current which is measured at the gate electrode. Therefore, to get the correct value of the charge fluence, the measured or external value must be corrected by accounting for the displacement components. The total current density measured in the external circuit J_{ext} is given by

$$J_{\text{ext}}=J_p+J_{\text{cap}}+J_{\text{ch}} , \tag{10}$$

where J_p is the actual injected photocurrent density (i.e., the particle current density), J_{cap} the capacitive displacement current density due to the changing applied bias, and J_{ch} is the displacement current density due to the charging of the traps. The capacitive displacement current is simply given by

$$J_{\text{cap}}=-C\frac{dV_a}{dt} , \tag{11}$$

where C is the dielectric capacitance of the SiO_2 film per unit area and dV_a/dt is the rate of change of the bias applied to the gate electrode. The displacement current density due to the charging in the SiO_2 is given by[31]

$$J_{\text{ch}}=e\left[1-\frac{\bar{x}}{d_{\text{ox}}}\right]\int_0^{d_{\text{ox}}}\frac{\partial n_t(x,t)}{\partial t}dx$$

$$=\left[1-\frac{\bar{x}}{d_{\text{ox}}}\right]\frac{dQ(t)}{dt} . \tag{12}$$

The actual particle current density is then given by

$$J_p\approx J_{\text{ext}}+C\frac{dV_a}{dt}-\left[1-\frac{\bar{x}}{d_{\text{ox}}}\right]\frac{dQ(t)}{dt} . \tag{13}$$

For electron trapping in SiO_2, both displacement currents are often neglected[13,14,21,23,31,32] since they are usually much smaller than the set current level, particularly for samples with low trapping probabilities ($\lesssim 0.1$). (The trapping probability is simply the probability of an electron becoming trapped as it traverses the length of the SiO_2 film. This probability can be calculated by the multiplication of the density of the empty traps by the capture cross section. Typically, for thermally grown oxides, the trapping probability is of the order of 10^{-6}–10^{-5}.) In our case, the external current and the total of the displacement currents were of the same order of magnitude, at least during the initial portion of the experiment. Therefore the displacement current components were calculated and subtracted from the current measured in the external circuit to obtain the actual particle current density and subsequent charge fluence.

The solution of Eq. (5) yields an exponential time dependence of the trapped charge, Q, from which σ may be deduced. This is the most common procedure for determining σ from charge trapping measurements.[1,13,14,23,32,33] However, there are experimental limitations to this technique. First, one assumes that the average electric field (F) is constant throughout the experiment. If large changes in the field arise from significant charge trapping, inaccurate values may result. For small amounts of trapped charge (and therefore small midgap voltage shifts), the average field may be assumed to be constant and the exponential fit will produce accurate values of σ. It must also be assumed that the particle current is constant in time to properly use the exponential fit. Again, for small densities of Coulombic centers this is true.

In the present work, the samples purposely contained large densities of traps which resulted in large midgap voltage shifts and an average field that was time dependent. Also, substantial displacement currents were measured resulting in a particle current that was not constant. However, using Eqs. (7) and (8), the *instantaneous* effective cross section could be calculated since both the particle current and average field are known for all times. This procedure not only yielded accurate results, but produced a series of σ-F data points as opposed to a single data point from the exponential fit technique.

V. EXPERIMENTAL RESULTS AND DISCUSSION—COULOMBIC-ATTRACTIVE CENTERS

Figure 1 shows an example of data illustrating the measured midgap voltage shift (ΔV_{mg}) as a function of time during the avalanche injection of holes and subsequent photoinjection of electrons. In Figs. 2(a) and 2(b), the midgap voltage shift (ΔV_{mg}) and the applied gate voltage are shown in more detail for (a) the avalanche injection of holes (ΔV_{aval}) and (b) the internal photoemission of electrons electrons (ΔV_a). The reader should note that the bias applied during internal photoemission V_a is negative (i.e., electrons are injected from the gate contact).

As shown in Fig. 2(a), during the avalanche injection of holes, the midgap voltage shifts to greater negative values, demonstrating the increase in the total amount of

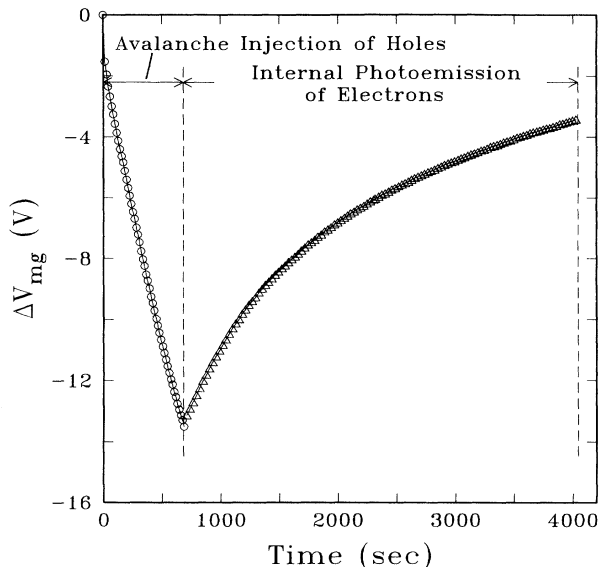

FIG. 1. Midgap voltage shift ΔV_{mg} for avalanche injection of holes from the silicon substrate and their subsequent trapping on the As-related sites in the SiO_2 layer, followed by internal photoemission of electrons from the Al gate and their subsequent annihilation of the trapped holes as a function of time.

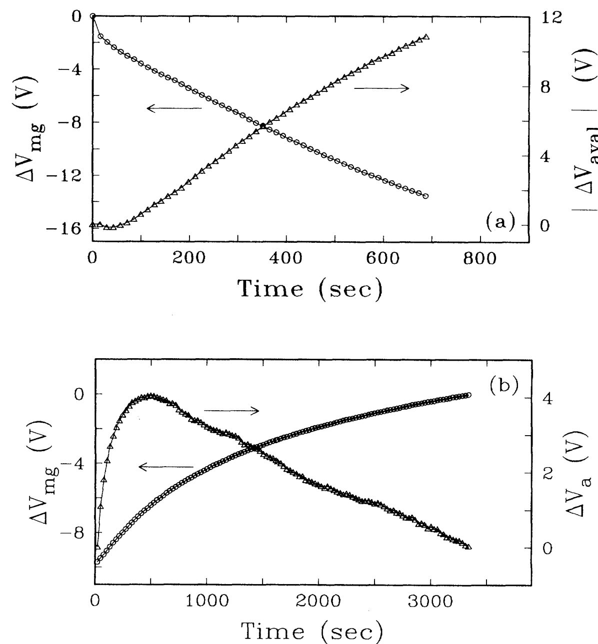

FIG. 2. Typical midgap voltage and applied-gate-voltage shift characteristics during (a) avalanche injection of holes from the silicon into the SiO_2 film followed by (b) internal photoemission of electrons from the Al gate for Coulombic trapping centers created by the holes trapped on the As-related sites. V_{aval} is the peak voltage of the sawtooth wave form applied to the gate electrode for the avalanche injection (a) while for the internal photoemission (b), V_a is the (negative) dc bias applied to the gate electrode.

positive charge in the SiO_2 film. No analysis was performed on the trapping parameters of the injected holes. *The injection of the holes was used only as a technique to create Coulombic trapping sites (for electrons) in the SiO_2 film.* After the Coulombic trapping sites were introduced, electrons were photoinjected into SiO_2. Figure 2(b) shows the midgap shift returning to lower negative voltages as some of the electrons are captured on the Coulombic sites. The applied voltage is also shown to change with time.

Figure 2(b) demonstrates the phenomenon called *voltage turnaround.* One might normally assume that as the density of trapped electrons in the SiO_2 film increased, the magnitude of the average electric field and the applied voltage should increase in time. This, however, is not the case as shown in Fig. 2(b) where the voltage magnitude decreases initially and then after a substantial period of time, increases. This phenomenon has been noted for both electron[13,32] and hole[14,33] trapping and is due to the experimental technique that is used to inject the charge carriers. In our case, a feedback system is used to maintain a constant, *externally measured current.* The applied voltage is adjusted to keep this current constant. However, there is a displacement current which is due to the changing charge state of the SiO_2 film [see Eq. (13)]. The displacement current arises from the trapping rate of electrons. Initially the density of unfilled traps (i.e., Coulombic centers) is very large, and since the trapping rate is proportional to the density of unfilled traps, the displacement current density (J_{ch}) is also large. To maintain a constant external current, the magnitude of the applied voltage is increased. The changing applied bias also contributes a term to the displacement current. However, it should be stressed that this is only a consequence of the trapping rate and the condition of a constant current in the external circuit. As time increases, the density of trapping centers decreases, thus reducing the trapping rate and displacement current. Eventually, the displacement current becomes smaller than the value set for the external current and the voltage turnaround occurs. Beyond the voltage turnaround, the applied bias changes, not in response to the changing displacement current, but rather in response to the buildup of trapped charge in the SiO_2 film.

The time at which the voltage turnaround occurs is a complicated function of the density and spatial location of traps, the external current level, as well as the initial applied voltage. All of these parameters affect the trapping rate by altering the density of traps, by changing the capture cross section (which is strongly field dependent), or simply by altering the external current value. It is not important to know the exact nature and effects of these parameters on the turnaround voltage. We know the applied bias and can calculate the density of trapped electrons, and therefore the trapping rate at any point in time. Since we can deduce the displacement current from measured quantities, we can calculate the actual particle current as a function of time [see Eq. (13)]. It is from the particle current that the charge fluence is calculated. Figure 3 shows an example that demonstrates this point. This figure shows the displacement currents and calculated particle current (I_p) as a function of time, where the changing applied bias is shown in the inset. Even though the major contribution to the displacement current arises from the changing applied bias, it should be stressed that this is only a result of the changing trapping rate and the need to maintain a constant current in the external circuit. The two displacement currents are separated only for clarity.

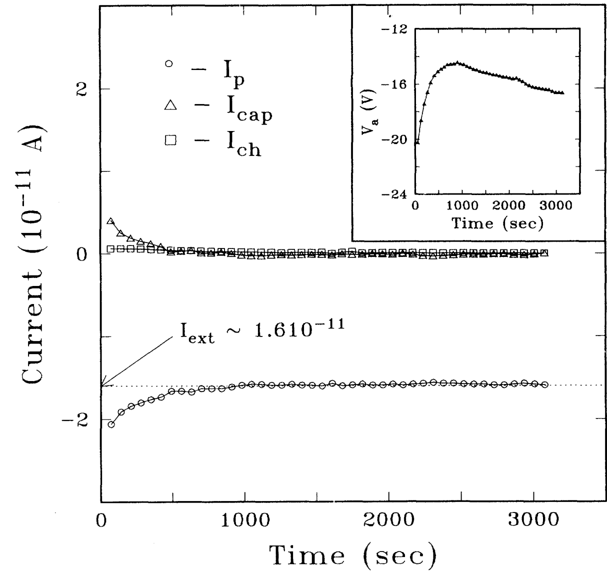

FIG. 3. Transient current characteristics separating the displacement current ($I_{ch}+I_{cap}$) from the particle current I_p. The external current I_{ext} was set to be constant, while I_{cap} is calculated from the changing applied bias (see inset) and I_{ch} is calculated from the trapping rate of electrons.

Using Eq. (7), the effective capture cross section is calculated from the rate of change of trapped charge per unit area Q with respect to the total charge fluence N_{inj}. Figure 4 shows examples of the trapped charge as a function of the total injected charge for four different values of electric field. It should be noted that the values of electric field given here are only *averages* as the applied bias changes with time. This figure demonstrates the effect of the electric field on the density of trapped charge for a given charge fluence.

From the data shown in Fig. 4, a derivative at each point was determined and σ was calculated using Eq. (7). Even though the applied bias changes during the experiment, it is known at every point in time. Therefore σ can be evaluated as a function of the average electric field. Numerous experiments were carried out where the externally applied field, the density of Coulombic trapping centers, and the external current were varied. For each experiment, a series of σ values was determined. Finally, the data from all the experiments were grouped into small intervals of average electric field ($\Delta F \lesssim 1\times10^5$ V/cm) and an average over the interval was taken. Figure 5 shows the effective capture cross section as a function of the electric field. Each data point shown here represents an average of all data values within the range ΔF. (Error bars have not been included for these data

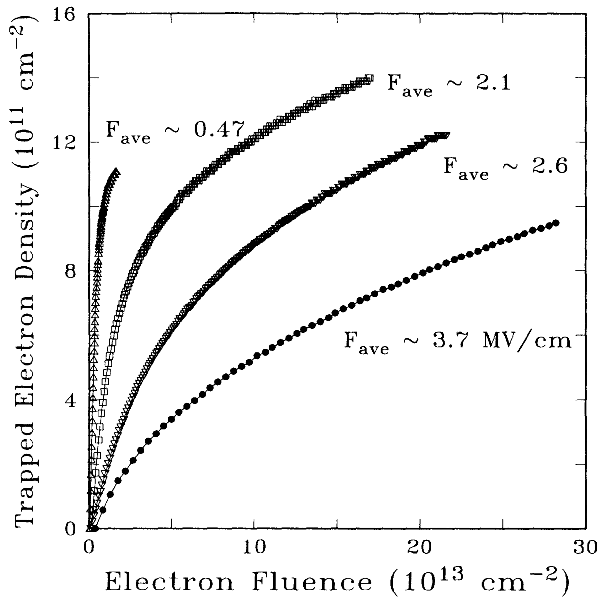

FIG. 4. Typical room-temperature trapping characteristics for Coulombic centers. The injected charge fluence is calculated from the net particle current I_p. The values of F given here are actually the time-averaged values since the electric field changes as electrons are trapped.

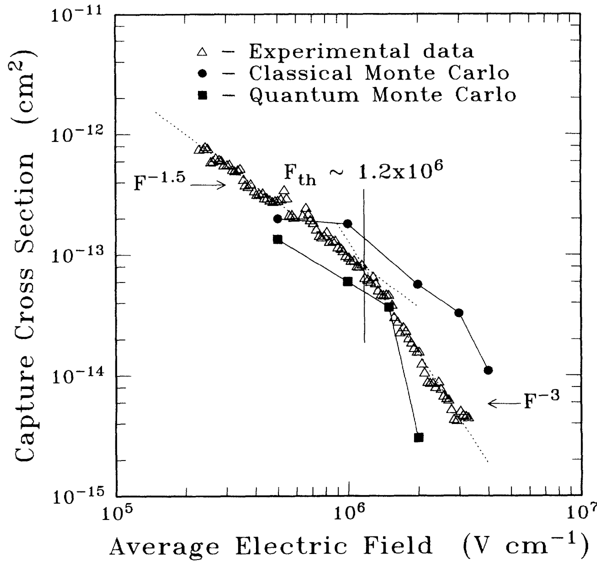

FIG. 5. Coulombic capture cross section as a function of the average electric field. A power-law fit for the low- and high-field regions is shown and gives exponents $n=-1.5$ and -3.0, respectively. The threshold F_{th} is found to be $\sim 1.2\times10^6$ V/cm. Also shown are both quantum and classical Monte Carlo simulations. Both models include the effects of electron heating. The quantum calculation also includes both the existence of and transitions (phonon and photon) between bound states of the trap potential and tunneling from these levels into the SiO_2 conduction band. The experimental data fall between these models, implying that both electron-heating effects and quantum-mechanical tunneling contribute to the decrease in σ in the high-field regime.

since the errors are smaller than the symbols shown.) It can be seen that σ falls into two distinct regions of average electric field with the threshold $F_{th}\approx 1.2\times10^6$ V/cm. A power-law fit was calculated ($\sigma \propto F^n$), and the exponents (n) are approximately -1.5 and -3.0 for the low- and high-field regions, respectively.

These values of n are in agreement with Ning's earlier work[23] even though there are a number of differences in both the samples and the analytical and measurement techniques. The Coulombic centers in the devices used in the present study were generated using ion implantation of As^+ and as such were positioned away from either interface ($\bar{x}/d_{ox}=0.38$, measured from the Al-SiO_2 interface using the photo I-V technique[13,14,32,34]). Not only was the charge density larger (and controllable), but the position of the trapped charge centroid was measured experimentally. Subsequently, the voltage shifts measured in this work were approximately two orders of magnitude larger. As a result of both the large initial displacement current and the relatively large density of Coulombic centers, the applied voltage (therefore average field), changed substantially throughout the measurement. This not only led to a greater number of data points, but also allowed a cross check between data taken with different densities of Coulombic centers produced though the avalanche injection of holes, different initial applied bias, and different injected current densities.

In the low-field regime, the dependence of σ on the field F is usually attributed to Poole-Frenkel (PF) lowering of the potential barrier surrounding the Coulombic center [see Eqs. (A1)–(A3) in Appendix A]. It can be shown that the PF lowering of the potential around a Coulombic trap leads to an $F^{-1/2}$ dependence of the critical radius r_c, where r_c is the distance along the field direction from the trap center to the potential maximum. For low electric fields, where the distortion of the potential on either side of the trap is still relatively small, the *capture volume* is proportional to r^3. Therefore the capture probability and cross section are proportional to $F^{-3/2}$ in the low-field regime. This simple calculation applies only if two assumptions are made. First, the volume of the trap must be a sphere of volume $4/3\pi r_c^3$ and second, the critical radius r_c must be taken as the distance from the center of the trap to the PF-lowered potential maximum along the direction of the externally applied field. With these assumptions, the capture volume varies with the field as F^n where $n=-\frac{3}{2}$. However, the capture volume is not a sphere as the trap potential is perturbed by the field and a spherical geometry would only apply with $F=0$. Also, according to Lax,[35,36] final capture occurs only after an electron falls below some critical energy where the probability of being remitted is equal to the probability of final capture. If some value below the potential maximum is used to define the critical energy below which an electron is considered trapped, the critical radius of this point (from the trap center) does not vary with an $F^{-1/2}$ dependence and will not yield a capture volume dependence of $F^{-3/2}$. [This simple calculation may be performed with the suitable algebraic manipulations of Eqs. (A1) and (A2) in Appendix A.]

Dussel and Böer[37] assumed an electron to be captured

once it was 2 kT below the top of the PF-lowered barrier and calculated the "actual" (not spherical) volume enclosed by the trap potential giving a full description of the *volume shrinkage* (VS) model including the effects of the Poole-Frenkel lowering of the barrier. However, even Ning's corrected version[38] of the VS model equations, underestimates the field exponent (n), even in the low-field regime. Therefore, for $F < F_{\text{th}}$, the field dependence of the capture probability (and therefore the capture cross section) arises from more than just the volume shrinkage of the trap and PF lowering of the trap potential.

Once the average field rises above $F \gtrsim F_{\text{th}}$ [$\sim(1-2)\times 10^6$ V/cm], at least two different phenomena can contribute to the decrease in the capture cross section as shown in Fig. 5. The most obvious of these is quantum-mechanical tunneling. As the average electric field increases, the distance from the center of the trap to the edge of the conduction band (along the direction of the field) decreases and therefore, the electron tunneling probability increases and the effective capture cross section decreases. A relatively simple calculation shows that tunnel detrapping from shallow excited states of the trap site (even for fields as low as 10^5 V/cm) can be significant and does contribute to the determined value of σ; therefore σ can decrease more rapidly with F than the VS model predicts, even for $F < F_{\text{th}}$.

Heating of the electron distribution with increasing electric field can also cause a decrease in the electron trapping probability and the effective capture cross section in the high-field regime. As first suggested by Dussel and Böer,[37] and demonstrated by Ning,[23] when the electron distribution becomes hot with respect to the SiO_2 conduction-band edge, the capture of an electron results from increasing energy loss through phonon and/or photon-assisted processes. Therefore a corresponding decrease in the trapping probability and capture cross section would be found with the increasing average electron energy. Ning[23] assumed a Maxwell-Boltzmann distribution of electron energies from which an effective electron temperature was calculated. He further assumed that the average electron temperature was proportional to the average (external) applied field. Finally, using Lax's[36] cascade capture model, assuming electron capture through acoustic phonon emission and combining this with the VS model, he showed that σ should vary with F^{-3}. He also showed qualitative agreement between this model and his data. The power factor value of $n = -3$ agrees with the results of the present work. However, it is now known[26–30] that the *hot* electron distribution is not governed by a Maxwell-Boltzmann distribution of energies and even though the average electron energy is proportional to F in the range $1 \lesssim F \lesssim 4$ MV/cm, recent results[26–30] have shown both acoustic and optical phonons are important in the electron scattering in the high-field regime. Therefore it would seem that Ning's[23] result ($n = -3$ in the high-field regime) although correct, was somewhat fortuitous. In the following paragraphs we shall present a comparison between Monte Carlo simulations and the experimental data. Since the Monte Carlo model has been found[26–30] to give an accurate representation of the electron-energy distribution, no attempt has been made to determine an *analytical* solution to the relationship between σ and F.

As the field increases, volume shrinkage of the Coulombic trap decreases the effective capture probability and therefore the capture cross section. This effect, along with quantum-mechanical (QM) tunneling dominate the change in σ in the low-field regime. Electron scattering for fields $F \lesssim F_{\text{th}}$ is controlled by polar optical phonons which effectively thermalize the electrons such that their average energy is small relative to the SiO_2 conduction-band edge. As the field approaches F_{th}, the nonpolar acoustic phonons begin to dominate the scattering process. The acoustic phonon scattering process results in small electron-energy losses, but in large-angle scattering events. Therefore as electrons gain energy from the field, their effective path length in the SiO_2 films becomes longer and their transport becomes dispersive. The continuing high rate of energy loss due to optical phonon scattering keeps the average electron energy from "running away." The increased electron energy reduces the effective capture probability since the electrons must now lose significantly more energy to become trapped. The electrons, however, also have longer paths while traversing SiO_2 films, which allows each electron more "passes" at a single trap (see Fig. 12 in Ref. 24) and thus increases the effective capture cross section. Since these two effects affect the capture probability with opposing field tendencies, one or the other of these phenomena will tend to dominate in the high-field regime. For the Coulombic traps, these effects are presented in the following paragraphs of this section. For the neutral traps, a more detailed discussion is presented in Sec. VI.

Figure 5 shows a comparison between the experimental data and two different Monte Carlo simulations. The classical Monte Carlo model includes the effects of electron heating and treats the traps as ideal Coulombic potential wells. In this model, the electron motion is followed classically inside the potential well and electrons are considered trapped when their energy falls about $10\hbar\omega_{\text{LO}}$ ($\hbar\omega_{\text{LO}}=0.153$ eV, the optical phonon energy) below the local potential maximum around each trap.

In an attempt to avoid the difficulty of treating electrons classically when they are confined only a few nanometers away from the Coulombic center, we have also employed a quantum-mechanical model (referred to as the QM Monte Carlo model) which describes the electronic states in the well as Stark-shifted, hydrogenic levels for Coulombic-attractive potentials,[39–41] as described in Appendix A. We should stress the fact that we have no knowledge of the detailed structure of the potential very close to the As^+ core. Thus the electronic wave functions in the deep bound states might be poorly approximated. Fortunately, as long as the decay of the electrons from excited states to the trap ground state is faster than any other process involved, a detailed knowledge of the energy levels of the trap core is not needed to compute the *sticking probability*.[36] (The sticking probability S_υ, is the probability that an electron entering the trap at E_υ, will be finally trapped into the ground state of the trap, as explained in Appendix A.) We should also note that a significant statistical noise

affects the accuracy of the QM Monte Carlo results, mainly because of the long simulation time required to perform the ensemble average of the trap distributions, as explained at the end of Appendix A: the data shown in Fig. 5 obtained from the QM Monte Carlo model should not be considered more accurate than a factor of 2. Despite this, quantum-mechanical effects exhibit a qualitative trend which is well within our confidence level, showing a smaller cross section than predicted by the semiclassical model as well as faster decay at large electric fields.

A schematic diagram of the quantum-mechanical treatment of the Coulombic trap is shown in Fig. 6. This figure demonstrates, qualitatively, the processes that are included in the QM Monte Carlo simulation. Shown schematically (not to scale) are the Stark-shifted hydrogenic levels $(E_1, E_2, \ldots, E_n)$ where the electrons are bound into localized states. The trap level E_t is defined by the Poole-Frenkel lowered potential maximum, and E^* is the lower limit of the pseudocontinuum of states defined in Appendix A, and is the highest level we consider as a "localized" quantum level. Finally, we include the transitions from any localized state to any other via phonon and photon interactions as well as transitions into the conduction band via quantum-mechanical tunneling for all states except the ground state of the trap.

Figures 7(a), 7(b), and 7(c) show the detailed structure of the excited and bound states of a Coulombic trap for the $F=3\times10^5$ V/cm (the low-field case), 1.7×10^6 V/cm $(F\sim F_{th})$, and 5×10^6 V/cm (the high-field case), respectively. For the structure shown in Fig. 7(a), the electrons are not hot and their average energy is within a few kT of the SiO_2 conduction-band edge. For this case, the trapping probability is determined mostly by the gross features of the Coulombic trap (i.e., the volume shrinkage and the Poole-Frenkel lowering of the trap depth) and tunneling from the bound states into the SiO_2 conduction band. For the high-field case [Fig. 7(c)], the average electron energy is now $\gg$kT with respect to the SiO_2 conduction-band edge. In this high-field regime, there are three phenomena which directly affect the capture cross section: (i) the increasing average electron energy (which decreases σ with increasing F), (ii) the longer effective path length (which increases σ with increasing F), and (iii) the increasing quantum-mechanical tunneling probability (which decreases σ with increasing F). One must also note that even though σ decreases more rapidly for $F>F_{th}$ than for $F<F_{th}$, the volume shrinkage of the trap still occurs in the high-field regime. Therefore the three phenomena mentioned above are those that could cause the "change" in the σ-F characteristic for $F>F_{th}$ (i.e., the increase in n from $-\frac{3}{2}$ to -3). Since the longer electron path length is the only phenomenon that increases σ, it is evident the either the "hot" electron distribution or the increased tunneling (or both) cause the increase in the exponential factor, n for $F>F_{th}$.

In Fig. 8, we show the probabilities associated with quantum-mechanical tunneling from the bound excited states of the trap, thermal reemission into the conduction band and the *sticking probability* of the traps as a function of the externally applied field. It should be noted that even for low fields, the tunneling probability is still significant and for larger fields this probability ap-

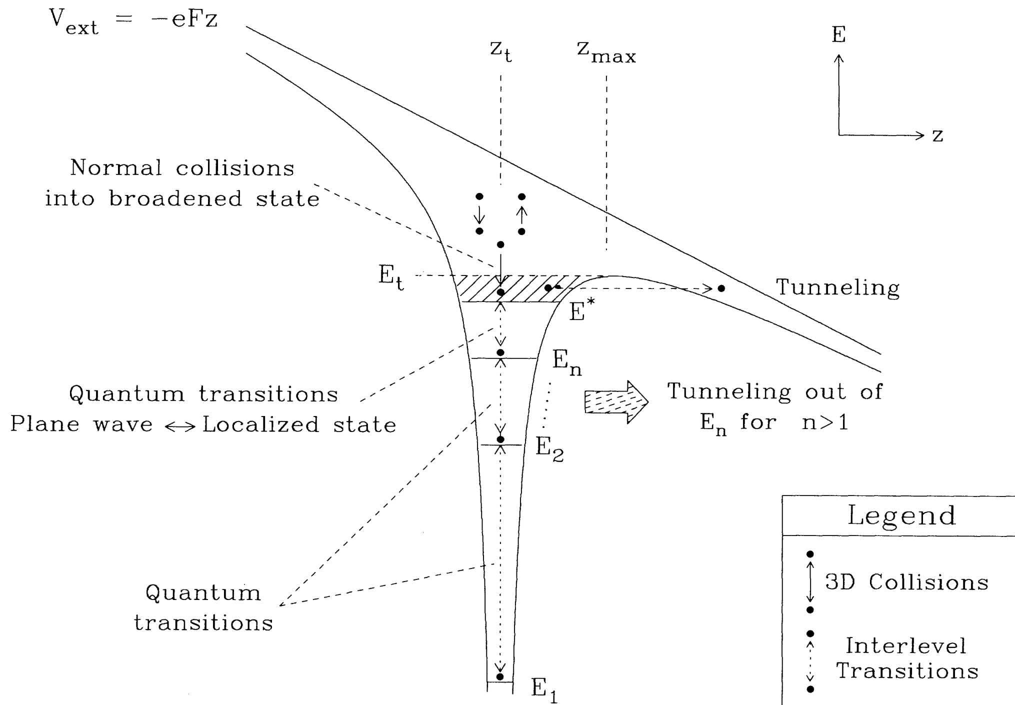

FIG. 6. Schematic diagram of the trap potential under the influence of an externally applied electric field. Shown here are the possible electronic transitions that occur within the trap from interactions of electrons with phonons and photons.

proaches one. The *structure* shown in the electron trapping probabilities shown in Fig. 8 (particularly for the thermal reemission probability curve) is not an artifact but results from the movement of the Stark-shifted levels with increasing electric fields. Finally, it should be stressed that the transition of the sticking probability from low to high fields is extremely sharp and large (approximately five orders of magnitude) and is due to the disappearance of excited bound states in the Coulombic well connected to the continuum via phonon emissions. Quantitatively this transition occurs at the heating threshold of the electron distribution. This must be viewed as a fortuitous accident which makes us unable to separate clearly the role of electron heating from the structure of the excited states in the trap.

For the case of the Coulombic centers, we have found the low-field capture cross-section dependence on the electric field results from volume shrinkage, Poole-Frenkel lowering of the potential barrier, as well as from quantum-mechanical tunneling from the shallow excited trap states into the SiO_2 conduction band. For $F > F_{th}$, the effective electron path length increases, relative to the low-field case, which could make the reduction in σ as a function of the increasing field less pronounced. We must also include the effects of QM tunneling in this regime, as the tunneling probability approaches 1 for $F > F_{th}$. Therefore we surmise that the value of n for $F > F_{th}$ results from the increasing average electron energy compounded by QM tunneling from the bound states of the trap into the SiO_2 conduction-band edge.

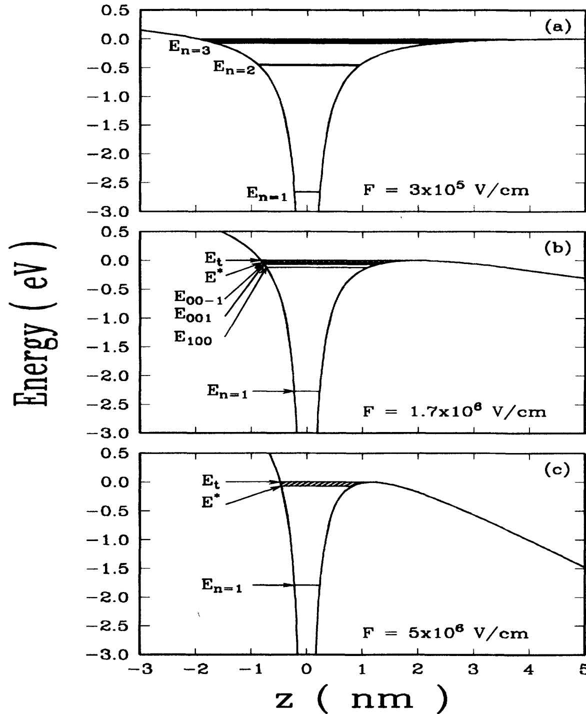

FIG. 7. Electronic structure of the Coulombic trap potential well for (a) $F = 3\times10^5$ V/cm (the low-field case), (b) 1.7×10^6 V/cm ($F \sim F_{th}$), and (c) 5×10^6 V/cm (the high-field case). The Stark-shifted bound and excited levels of the trap potential well are also shown. In the low-field regime (a), the average electron energy is within a few kT of the conduction band edge while for $F > (1-2)\times10^6$ V/cm the electrons are hot with respect to the conduction-band edge.

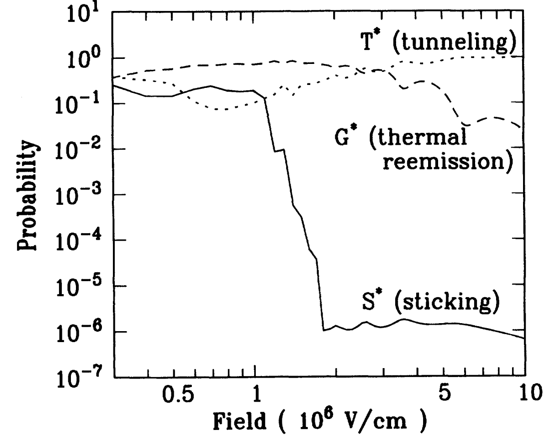

FIG. 8. In this figure the trapping probabilities associated with quantum-mechanical tunneling and thermal reemission of trapped electrons are shown as a function of the average electric field. Also shown is the effective *sticking probability* of an electron to the traps over the same field regime. For the case considered here involving the level E^*, the tunneling probability (T^*) is the probability that an electron at E^* will tunnel from this state into the SiO_2 conduction band. Likewise G^* is the probability that an electron at E^* will absorb a phonon and be reemitted from the trap. The sticking probability is the probability that the an electron entering the trap at E^* will be trapped into the ground state of the trap. Similar probabilities (not shown here) are calculated for each bound state E_ν, where an electron may initially enter the trap. These probabilities are stored in look-up tables and are used in the MC simulation once an electron enters the trap at any energy level E_ν.

VI. EXPERIMENTAL RESULTS AND DISCUSSION—NEUTRAL CENTERS

Arsenic-related trapping sites are amphoteric and are able to trap both electrons and holes.[13,14] For studying Coulombic centers in SiO_2, holes were trapped on the As-related sites, producing Coulombic-attractive centers for electrons. For the neutral traps, the experimental procedure is simpler since the avalanche injection of holes is not required. For both the Coulombic and the neutral traps, similar analytical techniques were used.

The general solution to Eq. (4) yields an exponential time dependence of the trapped charge,[21] which when combined with Eq. (8) gives

$$\Delta V_{mg} = \sum_i V_i \left[1 - \exp\left[\frac{-t}{\tau_i} \right] \right] , \tag{14}$$

where $V_i = e\bar{x}N_i/\epsilon_{ox}$, $\tau_i = (J\sigma_i/e)^{-1}$, and N_i and σ_i are the density and cross section of the ith type of trap, respectively. This assumes, of course, the presence of a number of different types of traps. If a fit using Eq. (14) is performed, the values of V_i will yield the density of

each particular trap. In our case, one dominant neutral trap could be distinguished from the midgap voltage shift characteristic. The density of the neutral centers was determined from a exponential fit of the measured midgap voltage shift. It was found that the density of-neutral centers measured (after correction for the position of the trapped charge centroid) was comparable to the implanted As^+ ion fluence.

Figure 9 shows a typical example of the midgap voltage shift as a function of time for the neutral traps. Since the trapping rate of the neutral centers was generally much smaller than that of the Coulombic centers, the displacement current was small and the voltage turnaround phenomenon was not seen. As shown, the midgap voltage shifts to higher positive voltage as the electrons are trapped on the neutral sites. The average electric field F increases as expected as the density of trapped charge in SiO_2 film increases.

After the determination of the density of the neutral traps using Eq. (14), the neutral capture cross section σ_n was calculated using Eqs. (7) and (8) in a similar manner to the procedure used for the Coulombic traps. Figure 10 shows σ_n as function of F. Also shown in this figure, for comparison, is a classical Monte Carlo[24] calculation which assumes a dipole $1/r^4$ potential for the neutral trapping center[36] and neglects tunnel detrapping. The error bars shown for the experimental data represent the mean-square error of F and σ_n for a large number of data points (~ 240). A quantum Monte Carlo simulation for the neutral trapping centers was not attempted due to the immense computation time that would have been necessary to acquire reasonable trapping statistics.

The most striking feature of the experimental data shown in Fig. 10 is that σ_n is approximately constant with F ranging from 5×10^5 V/cm to 6×10^6 V/cm. The classical Monte Carlo model (see Appendix B) predicts a slow rise in σ_n once the field becomes larger than the electron-heating threshold. The potential well for the neutral traps is much sharper than that of the Coulombic well and as such shows little or no change in σ_n resulting from volume shrinkage of the trap. It is not surprising that the low-field values of σ_n appear independent of F. As mentioned in Sec. V, for $F > F_{th}$ the conduction electrons become hot and their transport becomes dispersive due to the large-angle electron scattering interaction cause by the nonpolar acoustic-phonon modes. As a result, their effective path length increases. The classical Monte Carlo simulation includes the electron heating effects, and for $F > F_{th}$ shows σ increasing. However, the experimental data are relatively constant (see Fig. 10). The difference between the experimental data and the classical simulation is not a result of the longer path length nor a result of the hot electron distribution. Only QM tunneling is not included in the model and since tunneling would cause a decrease in σ_n (for a given F), it is probable that this is the reason for the differences between the Monte Carlo model and the experimental data.

Other work on neutral traps in SiO_2 include x-ray induced centers,[31,42] electron-beam-induced defects,[43] so-called "intrinsic" centers,[1,2] and "hot-electron" induced centers.[1-12] Generally, no strong field dependence of the neutral cross section has been noted independent of the technique used to induce these traps. However, the magnitude of the neutral cross section has been found to vary from $\sigma_n \sim 1\times10^{-18}$ to 1×10^{-15} cm^2 depending upon the nature of the defects. For the electron beam irradiated

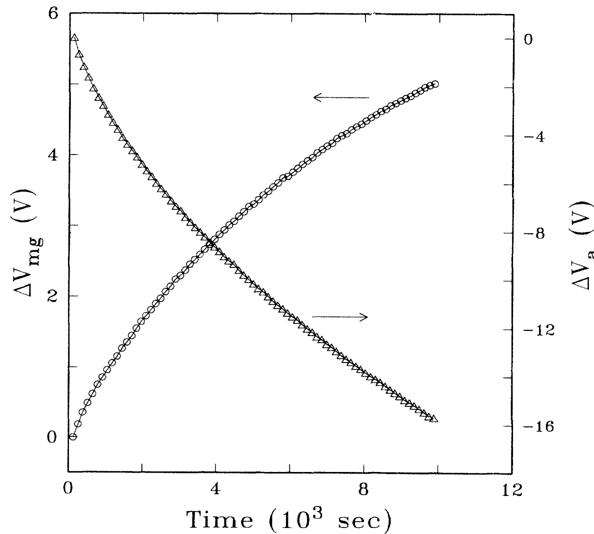

FIG. 9. Typical midgap voltage shift ΔV_{mg} and applied voltage shift ΔV_a characteristics during internal photoemission of electrons from the Al gate and their subsequent trapping on the neutral As-related sites in the SiO_2 film as a function of time.

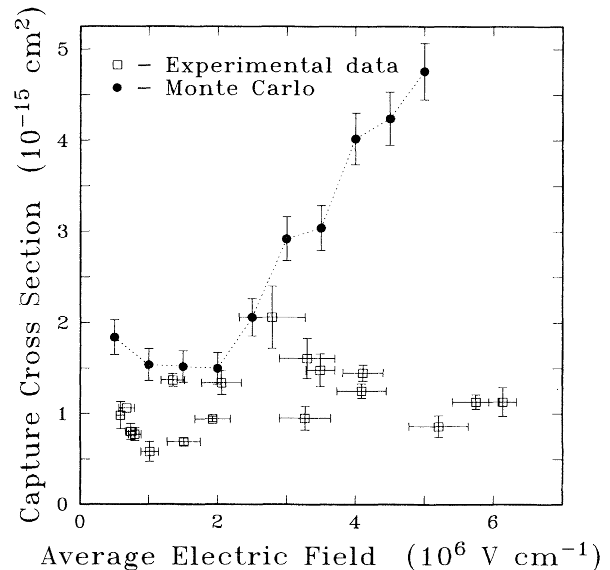

FIG. 10. Capture cross section as a function of the average electric field for the neutral traps. Included are the results from the classical Monte Carlo (Ref. 28) calculations (●) where tunnel detrapping has *not* been included. The error bars shown for the experimental data (□) are the mean-square error of the average electric field and the capture cross section over a large number of data points (~ 240).

samples,[43] an exponential dependence of σ_n on the average electric field was found ranging from $\sigma_n \sim 1\times10^{-15}$ cm^2 at 5×10^5 V/cm to $\sigma_n \sim 2\times10^{-16}$ cm^2 at 3×10^6 V/cm. Although this variation is not large, an exponential fit seems to be appropriate for these data. Intrinsic neutral centers[1,2] in SiO_2 have been reported with cross sections as small as $\sigma_n \sim 6\times10^{-19}$ cm^2.

It is obvious that the neutral trapping centers generated by different means (i.e., intrinsic, irradiation, field stressing, ion implantation, etc.) should not necessarily show the same capture cross sections since the microscopic details of the sites are probably different. Although a small field dependence of σ_n in one case has been reported,[43] other results[1,2,31,42] (including the present work) do not show this trend. The main conclusions that may be drawn in terms of the neutral centers is that the capture cross section is smaller and the field dependence is less pronounced than that of a Coulombic site. The lack of a strong field dependence is probably due to the much shorter effective range of the potential of the neutral trap.

VII. CONCLUSIONS

In MOS capacitors, trapping centers were introduced using ion implantation of As^+ into the SiO_2 film. With the avalanche injection of holes from the silicon, Coulombic trapping centers were produced on the As-related sites. Using photoinjection of electrons from the gate contact, and measuring the transient midgap voltage response, the capture cross section of the Coulombic centers have been determined for average electric fields ranging from 2×10^5 to 3×10^6 V/cm. In this range, σ varies from $\sim10^{-12}$ to $\sim3\times10^{-15}$ cm^2. A threshold in the average field (F_{th}) is found for the σ-F characteristic below which the power-law exponent is found to be -1.5. Above $F\sim1.2\times10^6$ V/cm, the power-law exponent is found to be -3.0. The low-field dependence is attributed to Poole-Frenkel lowering of the potential surrounding the trap in the direction of the field. However, quantum-mechanical tunneling is also significant for $F \gtrsim 10^5$ V/cm. Beyond F_{th}, electron heating becomes significant, and together with tunneling from bound and excited states of the trap potential into the conduction band of the SiO_2 is primarily responsible for the change in the power-law exponent of the σ-F characteristic.

Since the implanted As^+ produces centers that are amphoteric and subsequently trap both electrons and holes, similar experimental and analytical techniques were used to determine the neutral capture cross section (σ_n) as a function of the average electric field. It was found that σ_n is approximately constant at $\sim(1-2)\times10^{-15}$ cm^2 for an average electric field in the range of 5×10^5 to 6×10^6 V/cm.

In this experiment, the same trapping sites have been used to determine the field dependence of two different site potentials; namely Coulombic-attractive and neutral centers. With the use of ion implantation, the position and density of the sites could be controlled with great accuracy. In past studies, traps were induced through process variations and thus knowledge about their characteristics was somewhat limited. In this study, the dependence of trapping sites upon particular growth and processing conditions was eliminated. Thus a more complete and controlled set of data has been realized together with the best theoretical treatment of this problem to date, including carrier heating and quantum effects which have been neglected or not considered important in the past.

ACKNOWLEDGMENTS

The authors would like to thank R. F. DeKeersmaecker for supplying the samples, E. Cartier for many helpful discussions, and T. N. Theis for a critical reading of this manuscript.

APPENDIX A

In this appendix, we describe the approach taken to account for the quantized states in a Coulombic well and how this model has been incorporated into a Monte Carlo (MC) simulation (referred to as "QM Monte Carlo" in the text).

1. Quantum states in a Coulombic well

The potential of a Coulombic-attractive (positive) charge of a trap at $z=z_t$ in an external electrostatic field of strength F, along the z direction, is given as

$$V(z) = -eFz - \frac{e^2}{4\pi\epsilon_{ox}|z-z_t|} . \quad \text{(A1)}$$

With reference to Fig. 6, the local maximum of the potential is at

$$z_{max} = z_t + \left[\frac{e^2}{4\pi\epsilon_{ox}}\right]^{1/2} \frac{1}{F^{1/2}} . \quad \text{(A2)}$$

In the following, we will find it useful to define the "barrier lowering" term

$$\Delta\phi = \frac{e^{3/2}}{(4\pi\epsilon_{ox})^{1/2}} F^{1/2} . \quad \text{(A3)}$$

We use second-order perturbation theory to describe the Stark-shifted eigenvalues and the localized electronic eigenstates on the potential (A1) following the procedure of Beckenstein and Krieger.[39] The eigenvalues are labeled by quantum numbers (n_1,n_2,m), with $n=n_1+n_2+|m|+1$ replacing the "usual" principal quantum number n obtained in a spherically symmetric case ($F=0$). The energy of a level (n_1,n_2,m) is given by

$$E_n = E_t - \mathrm{Ry}_{ox}\left[\frac{1}{n^2} + 3n(n_1-n_2)\frac{F}{P} + \frac{n^4}{8}[17n^2 - 3(n_1-n_2)^2 - 9m^2 + 19]\left[\frac{F}{P}\right]^2\right] , \quad \text{(A4)}$$

where E_t is the local maximum of the potential (see Fig. 6) and

$$\mathrm{Ry}_{\mathrm{ox}}=\frac{e^2}{8\pi\epsilon_{\mathrm{ox}}a}\simeq 2.96\ \mathrm{eV}\ ,$$

$$a=\frac{4\pi\hbar^2\varepsilon_{\mathrm{ox}}}{e^2 m_{\mathrm{el}}}\simeq 1.13\ \text{Å}\ ,$$

$$P=\frac{e^5 m_{\mathrm{el}}^2}{(4\pi\epsilon_{\mathrm{ox}})^3\hbar^4}\simeq 523\ \mathrm{MV/cm}\ .$$

Here m_{el} is the free electron mass, which we use as an approximation to the electron effective mass at high energy, ϵ_{ox} is the high-frequency permittivity of the oxide ($\simeq 2.15\epsilon_{\mathrm{vac}}$),[23] e is the magnitude of the electron charge, $\hbar$ is the reduced Planck constant, a is the Bohr radius, and $\mathrm{Ry}_{\mathrm{ox}}$ is the ionization energy (Rydberg) in the unperturbed case. The eigenfunctions corresponding to the levels given by Eq. (A4), $\zeta_{n_1,n_2,m}$, are treated according to degenerate perturbation theory in the perturbing Hamiltonian $-eFz$. They are linear combinations of the hydrogenlike wave functions $\psi_{nlm}(r,\theta,\phi)$:

$$\zeta_{n_1,n_2,m}(r,\theta,\phi)=\sum_{n,l,m}\gamma_{nlm}^{(n_1n_2m)}\psi_{nlm}(r,\theta,\phi)\ , \qquad \text{(A5)}$$

the coefficients γ being obtained from degenerate perturbation theory. We shall be using levels only up to $n=3$. Explicitly, for the first eigenvalues and eigenfunctions (expressing the eigenvalues to first order for simplicity) we have for $n=1$,

$$E_1^{(0)},\quad \zeta_{000}=\psi_{100}\ ; \qquad \text{(A6a)}$$

for $n=2$,

$$\begin{aligned}
&E_2^{(0)}-3aeF,\quad \zeta_{100}=\frac{1}{\sqrt{2}}(\psi_{200}+\psi_{210})\ ;\\
&E_2^{(0)},\quad \zeta_{001}=\psi_{211}\ ;\\
&E_2^{(0)},\quad \zeta_{00\bar{1}}=\psi_{21\bar{1}}\ ;\\
&E_2^{(0)}+3aeF,\quad \zeta_{010}=\frac{1}{\sqrt{2}}(\psi_{200}-\psi_{210})\ ;
\end{aligned} \qquad \text{(A6b)}$$

and for $n=3$,

$$\begin{aligned}
&E_3^{(0)}-9aeF,\quad \zeta_{200}=\frac{1}{\sqrt{2}}\left[\psi_{310}+\frac{\sqrt{3}}{2}\psi_{300}+\frac{1}{2}\psi_{320}\right]\ ;\\
&E_3^{(0)}-\tfrac{9}{2}aeF,\quad \zeta_{101}=\frac{1}{\sqrt{2}}(\psi_{311}+\psi_{321})\ ;\\
&E_3^{(0)}-\tfrac{9}{2}aeF,\quad \zeta_{10\bar{1}}=\frac{1}{\sqrt{2}}(\psi_{31\bar{1}}+\psi_{32\bar{1}})\ ;\\
&E_3^{(0)},\quad \zeta_{002}=\psi_{322}\ ;\\
&E_3^{(0)},\quad \zeta_{110}=\frac{1}{\sqrt{2}}(\psi_{300}-\sqrt{3}\psi_{320})\ ;\\
&E_3^{(0)},\quad \zeta_{00\bar{2}}=\psi_{32\bar{2}}\ ;\\
&E_3^{(0)}+\tfrac{9}{2}aeF,\quad \zeta_{011}=\frac{1}{\sqrt{2}}(\psi_{31\bar{1}}-\psi_{321})\ ;\\
&E_3^{(0)}+\tfrac{9}{2}aeF,\quad \zeta_{01\bar{1}}=\frac{1}{\sqrt{2}}(\psi_{31\bar{1}}-\psi_{32\bar{1}})\ ;\\
&E_3^{(0)}+9aeF,\quad \zeta_{020}=\frac{1}{\sqrt{2}}\left[\psi_{310}-\frac{\sqrt{3}}{2}\psi_{300}-\frac{1}{2}\psi_{320}\right]\ ;
\end{aligned} \qquad \text{(A6c)}$$

where $E_n^{(0)}$ are the eigenvalues for the level n in the unperturbed case $E_n^{(0)}=E_t-\mathrm{Ry}_{\mathrm{ox}}/n^2$, and, as usual,

$$\psi_{nlm}(r,\theta,\phi)=R_{nl}(r)Y_{lm}(\theta,\phi)\ , \qquad \text{(A6d)}$$

with

$$R_{nl}(r)=\frac{-2}{(na)^{3/2}}\left[\frac{(n-l-1)!}{n(n+l)!}\right]^{1/2}\times\left[\frac{2r}{na}\right]^l e^{-r/na}L_{n-l-1}^{2l+1}\left[\frac{2r}{na}\right]\ ,$$

$$Y_{lm}(\theta,\phi)=(-1)^m\left[\frac{2l+1}{4\pi}\right]^{1/2}\times\left[\frac{(l-m)!}{(l+m)!}\right]^{1/2}P_l^m(\cos\theta)e^{im\phi}\ .$$

The functions $L_j^k(x)$ and $P_j^k(\mu)$ are the associated Laguerre and Legendre polynomial, respectively. Since perturbation theory fails at high "radial" quantum numbers,[40] we shall use the scheme above only for levels with $n<n^*$ such that

$$F\le F_{n^*}\ , \qquad \text{(A7)}$$

where F_{n^*} is the field at the classical turning point of the state with principal quantum number n^*. The condition (A7) implies that the highest level we shall consider as a localized quantum level of the trap has an energy

$$E^*=E_t-\Delta\phi\left[\sqrt{2}+\frac{1}{\sqrt{2}}\right]\simeq E_t-31.4\ \mathrm{meV}F^{1/2}\ . \qquad \text{(A8)}$$

The field F is expressed in MV/cm in the last expression. This corresponds to a quantum number n^* given by

$$n^*=\left[\frac{1\ \mathrm{Ry}_{\mathrm{ox}}}{E_t-E^*}\right]^{1/2}\simeq\frac{2.32}{F^{1/4}}\ . \qquad \text{(A9)}$$

with F again in MV/cm. States with energy $E_t>E>E^*$ will be treated as a pseudocontinuous band of plane waves of full width $\Delta E^*=E_t-E^*$. Note that (A9) implies that for $F\gtrsim 1.23$ MV/cm only one bound state exists in the well, which results in a sharp drop of the ability of the trap to capture electrons, as mentioned in the text.

We now have to consider the following processes (Fig. 10): (i) thermal (i.e., phonon-assisted) transitions between localized state ($\mu\rightarrow\nu$, $\mu\leftarrow\nu$), where μ and ν denote the sets of quantum numbers (n_1,n_2,m); (ii) thermal transitions between localized states and the band at E^*; (iii) thermal transitions between localized states and the three-dimensional continuum; (iv) thermal transitions between the pseudocontinuum at E^* and the three-dimensional continuum; (v) tunnel detrapping from localized and quasicontinuum states; (vi) optical transitions. Thermal processes (iii) and (iv) correspond to (temporary or virtual) trapping and detrapping processes. A process (v) corresponds to the total tunnel detrapping (or field ionization) of the trap. Optical processes are only significant when involving deep localized states.

2. Thermal transitions

We have considered phonon processes assisted by both acoustic and optical phonons, starting from the nonpolar Hamiltonian:

$$\mathcal{H}_{\mathbf{q}}^{\mathrm{ac}}(\mathbf{r},t)=i\left[\frac{\hbar}{2\rho\omega_{\mathbf{q}}}\right]^{1/2}e^{-i(\mathbf{q}\cdot\mathbf{r}+\omega_{\mathbf{q}}t)}Cq\ , \tag{A10}$$

where ρ is the density of the crystal, $\omega_{\mathbf{q}}$ is the frequency of a phonon with wave vector $\mathbf{q}$, and $C\simeq3.5$ eV is the coupling constant (deformation potential) for the electron-acoustic phonons interaction, and from the Fröhlich Hamiltonian

$$\mathcal{H}_{\mathbf{q}}^{(\mathrm{LO})}(\mathbf{r},t)=i\frac{eG}{q}e^{-i(\mathbf{q}\cdot\mathbf{r}+\omega_{\mathbf{q}}t)}\ , \tag{A11}$$

with

$$G=\frac{\hbar\omega_{\mathrm{LO}}}{4}\left[\frac{1}{\epsilon_\infty}-\frac{1}{\epsilon_0}\right],$$

for the interaction between longitudinal-optical (LO) phonons and electrons. Here ϵ_∞ and ϵ_0 are the optical and static permittivity, respectively, and ω_{LO} is the frequency of the LO phonons, having ignored their dispersion. The various transition rates have been calculated using the Fermi golden rule, but accounting for the finite lifetime of the levels by replacing the energy-conserving δ function with a Lorentzian. The "width" of the level is determined self-consistently as described below in Sec. A 5. Thus we have for the transition rate between the quantized levels μ and ν

$$\frac{1}{\tau_{AC}(\mu\to\nu)}=\frac{3g_\nu C^2}{4\pi^2\rho_>\omega_A}\times\begin{Bmatrix}n_A\\1+n_A\end{Bmatrix}\times\frac{\Delta E_\mu+\Delta E_\nu}{(\Delta E_\mu+\Delta E_\nu)^2+(\Delta E_\mu-\Delta E_\nu\pm\hbar\omega_A)^2}\times\int_0^\infty dq\,q^4|\langle\mu|e^{-i\mathbf{q}\cdot\mathbf{r}}|\nu\rangle|^2 \tag{A12}$$

(the upper symbols corresponding to absorption, the lower symbols to emission) where g_ν is the degeneracy of the νth level, ω_A is the acoustic-phonon frequency at the edge of the Brillouin zone (BZ) ($\omega_A\simeq c_s q_{\mathrm{BZ}}$, c_s being the sound velocity and q_{BZ} the wave vector at the edge of the BZ),[24] $\rho_>$ is the density associated to the heaviest ion in the Wigner-Seitz cell, n_A is the phonon population, and ΔE_μ is the width of the μth level. A factor of 3 accounting for the three acoustic branches has been introduced in (A12). Moreover, because of the larger contribution of large-q phonons in (A12), we have ignored the dispersion of the phonons and have considered only zone-edge modes. Similarly, for the polar transitions:

$$\frac{1}{\tau_{\mathrm{LO}}(\mu\to\nu)}=\frac{g_\nu e^2\omega_{\mathrm{LO}}}{4\pi^2}\left[\frac{1}{\epsilon_\infty}-\frac{1}{\epsilon_0}\right]\times\begin{Bmatrix}n_{\mathrm{LO}}\\1+n_{\mathrm{LO}}\end{Bmatrix}\times\frac{\Delta E_\mu+\Delta E_\nu}{(\Delta E_\mu+\Delta E_\nu)^2+(\Delta E_\mu-\Delta E_\nu\pm\hbar\omega_{\mathrm{LO}})^2}\times\int_0^\infty dq\,|\langle\mu|e^{-i\mathbf{q}\cdot\mathbf{r}}|\nu\rangle|^2\ . \tag{A13}$$

The thermal transitions from a localized level $(n_1,n_2,m)=\mu$ and the pseudocontinuum at E^* are given by

$$\frac{1}{\tau_{AC}(\mu\to E^*)}=\frac{3g^*C^2}{8\pi^4\rho_>\omega_A}\frac{(2m_{\mathrm{el}})^{3/2}(E^*)^{1/2}\Delta E^*}{\hbar^3}\times\begin{Bmatrix}n_A\\1+n_A\end{Bmatrix}\times\frac{\Delta E_\mu+\Delta E^*}{(\Delta E_\mu+\Delta E^*)^2+(\Delta E_\mu-\Delta E^*\pm\hbar\omega_A)^2}\times\int_0^\infty dq\,q^4|\langle\mathbf{k}^*|e^{-i\mathbf{q}\cdot\mathbf{r}}|\mu\rangle|^2\ , \tag{A14a}$$

$$\frac{1}{\tau_{\mathrm{LO}}(\mu\to E^*)}=\frac{g^*e^2\omega_{\mathrm{LO}}(2m_{\mathrm{el}})^{3/2}(E^*)^{1/2}\Delta E^*}{16\pi^4\hbar^3}\times\left[\frac{1}{\epsilon_\infty}-\frac{1}{\epsilon_0}\right]\times\begin{Bmatrix}n_{\mathrm{LO}}\\1+n_{\mathrm{LO}}\end{Bmatrix}\times\frac{\Delta E_\mu+\Delta E^*}{(\Delta E_\mu+\Delta E^*)^2+(\Delta E_\mu-\Delta E^*\pm\hbar\omega_{\mathrm{LO}})^2}\times\int_0^\infty dq\,|\langle\mathbf{k}^*|e^{-i\mathbf{q}\cdot\mathbf{r}}|\mu\rangle|^2\ . \tag{A14b}$$

where g^* is the degeneracy of the state n^* and $|\mathbf{k}^*\rangle$ is an approximation to the state at E^*, assumed to be a plane wave, normalized to the trap volume, with a wave vector $\mathbf{k}^*$. For $\mathbf{k}^*$ we take the expectation value $1/\hbar\langle n^*|\mathbf{p}|n^*\rangle$, where $\mathbf{p}$ is the momentum operator and $|n^*\rangle$ is the first-order eigenstate at E^* given by Eq. (A5). Finally, the thermal emission rates to the three-dimensional continuum are given by

$$\frac{1}{\tau_{AC}(\mu\to\mathbf{k})}=\theta(|E_\mu|-\hbar\omega_A)\frac{6\pi m_{\mathrm{el}}^{3/2}C^2(\Delta E_\mu)^{1/2}}{(2\pi\hbar)^3\rho_>\omega_A}n_A\times\frac{\int_0^\infty dq\,q^4|\langle\mathbf{k}|e^{-i\mathbf{q}\cdot\mathbf{r}}|\mu\rangle|^2}{\left\{\left[1+\left[\frac{E_{\mathbf{k}}-E_\mu-\hbar\omega_A}{\Delta E_\mu}\right]^2\right]^{1/2}-\frac{E_{\mathbf{k}}-E_\mu-\hbar\omega_A}{\Delta E_\mu}\right\}^{1/2}}\ , \tag{A15a}$$

$$\frac{1}{\tau_{\rm LO}(\mu\to\mathbf{k})}=\theta(|E_\mu|-\hbar\omega_{\rm LO})\frac{\pi m_{\rm el}^{3/2}e^2\omega_{\rm LO}(\Delta E_\mu)^{1/2}}{(2\pi\hbar)^3\left[\dfrac{1}{\epsilon_\infty}-\dfrac{1}{\epsilon_0}\right]}n_{\rm LO}\times\frac{\int_0^\infty dq\,|\langle\mathbf{k}|e^{-i\mathbf{q}\cdot\mathbf{r}}|\mu\rangle|^2}{\left\{\left[1+\left[\dfrac{E_{\mathbf{k}}-E_\mu-\hbar\omega_{\rm LO}}{\Delta E_\mu}\right]^2\right]^{1/2}-\dfrac{E_{\mathbf{k}}-E_\mu-\hbar\omega_{\rm LO}}{\Delta E_\mu}\right\}^{1/2}}, \quad \text{(A15b)}$$

where $|\mathbf{k}\rangle$ is a plane wave and $\theta(x)$ is the step function. Similar expressions hold from the transitions from the pseudocontinuum at E^*. The matrix elements occurring in (A8)–(A13) can be easily, but tediously, evaluated from the expressions (A6a)–(A6c).

3. Optical transitions

The optical transitions can be computed in the usual way from the Fermi golden rule and in the dipole approximation.[41] Thus

$$\frac{1}{\tau_{\rm opt}(\mu\to\nu)}=\frac{e^2(E_\nu-E_\mu)^3}{3\hbar^4c^3\pi\epsilon_{\rm ox}}|\langle\nu|\hat{\mathbf{r}}|\mu\rangle|^2, \quad \text{(A16)}$$

where c is the speed of light, and $\hat{\mathbf{r}}$ is the position operator. Similarly,

$$\frac{1}{\tau_{\rm opt}(E^*\to E_\mu)}=\frac{e^2(E^*-E_\mu)^3}{3\hbar^4c^3\pi\epsilon_{\rm ox}}\frac{E^{*1/2}\Delta E^*}{\hbar^3}\times(2m_{\rm el})^{3/2}|\langle\mathbf{k}^*|\hat{\mathbf{r}}|\mu\rangle|^2. \quad \text{(A17)}$$

4. Tunnel detrapping

We have followed Yamambe *et al.*[44] to obtain an expression for the rate of tunneling out of a localized level. Converting from their units, we obtain

$$\frac{1}{\tau_t(n_1,n_2,m)}=\frac{1}{\{n^3n_2!(n_2+|m|)!\}(\frac{1}{4}n^3\xi)^2\beta_2^{(0)}}\times\exp\left[3(n_1-n_2)-\frac{2}{(3n^3\xi)}\right]\times\frac{e^4m_{\rm el}}{(4\pi\epsilon_{\rm ox})^2\hbar^3}, \quad \text{(A18)}$$

where

$$\xi=\frac{(4\pi\epsilon_{\rm ox})^3\hbar^4}{e^5m_{\rm el}^2}F=\frac{F}{P},$$

$$\beta_2^{(0)}=n_2+\tfrac{1}{2}|m|+\tfrac{1}{2}.$$

5. Monte Carlo simulations

The major difficulty in treating the electron trapping process in a Monte Carlo (MC) simulation is the wide difference of time scales between the electron-transport phenomena and some of the processes described above. So, while it would be possible, in principle, to account for the transitions between trap states in the MC simulation of electron transport, this would require unreasonably long simulation times: for example, tunneling processes may require 10^{-8} sec, so that we would need carry on the simulation for at least 10^{-7} sec to determine whether an electron has been finally trapped in the ground state of the Coulombic well. In order to restrict the simulation times to the usual Monte Carlo time scale ($\sim 10^{-12}$ sec), we have chosen to proceed as follows.

In a Coulombic well in the presence of an external field only a finite number, K, fully localized states exist below the energy E^*. Let us order them in increasing energy and label them by the ordinary index i, running from 1 to K. Let us assume for now that electrons may be trapped by entering the band at E^* and possibly cascading into the ground state ($i=1$), assumed to be stable under tunnel detrapping and phonon emission. The occupation N_i of each level will be given by the first-order kinetic equations:

$$\frac{dN^*}{dt}=-\frac{N^*}{\tau^*}+\sum_{j=2}^{K}\frac{N_j}{\tau_p(E_j\to E^*)}+\Phi^*,$$
$$\frac{dN_i}{dt}=-\frac{N_i}{\tau_i}+\frac{N^*}{\tau_p(E^*\to E_i)}+\sum_{\substack{j=2\\ j\neq i}}^{K}\frac{N_j}{\tau_p(E_j\to E_i)}, \quad \text{(A19)}$$
$$\frac{dN_1}{dt}=-\frac{N^*}{\tau_p(E^*\to E_1)}+\sum_{j=2}^{K}\frac{N_j}{\tau_p(E_j\to E_i)},$$

where $\tau_p^{-1}(E_i-E_j)$ is the total interlevel rate for transitions assisted by both thermal and optical processes, and τ_i^{-1} is the total rate for leaving level i via tunneling, thermal, and optical processes to other levels. We shall also assume that $N_i \ll 1$, so that we shall not have to worry about the degeneracy of the levels. This is a reasonable assumption, as only one electron at a time will attempt to enter a given trap at the same time in a real situation. Finally, Φ^* is the supply function of electrons attempting to enter the trap via the band at E^* per unit time. This is provided by the MC simulation, as we shall describe below. At steady state (i.e., for time scales much longer than Φ^{*-1}),

$$\frac{dN_i}{dt}=0 \quad (i=2,K). \quad \text{(A20)}$$

Solving the system (A19) above with (A20), we obtain the steady-state values $\bar{N}_i$ for N_i and we can define the following quantities as $t \gg \Phi^{*-1}$:

$$S^*=\frac{\overline{N}^*}{\tau_p(E^*-E_1)}+\sum_{i=2}^{n}\frac{\overline{N}_i}{\tau_p(E_i\to E_1)}$$

(sticking probability) ,

$$T^*=\frac{\overline{N}^*}{\tau_t(E^*)}+\sum_{i=2}^{n}\frac{\overline{N}_i}{\tau_t(E_i)}$$

(tunnel-detrapping probability) ,

$$G^*=\frac{\overline{N}^*}{\tau_{\text{phonon}}(E^*\to 3d\ \text{continuum})}$$

(thermal-reemission probability) ,

which satisfy the obvious condition $S^*+T^*+G^*=1$.

The probabilities defined above express the conditional probability that an electron, having entered the pseudocontinuum at E^*, will be trapped into the ground state of the Coulombic well (S^*), will be thermally reemitted from any level (G^*), or leave the trap via tunneling out of any level (T^*).

The variables S^*, T^*, and G^* are obviously functions of the field acting on the Coulombic well, as the number of levels K and the energies $E^*, E_1, \ldots, E_K$ are functions of the external field. In a completely analogous way, we can consider the sticking (S_ν), tunnel-detrapping (T_ν), and thermal reemission (G_ν) probabilities for an electron entering the νth level, ν labeling the states (n_1, n_2, m), by considering a system analogous to Eqs. (A19), the supply function Φ_ν now "feeding" the νth level.

For the numerical implementation of this scheme in a MC simulation, we proceed as follows.

(i) We solve the system (A19) (and the analogous systems with the supply function feeding other localized states) for a set of external fields in the range 0.1–10 MV/cm by computing the scattering rates, as described in the preceding sections, and employing, for the widths ΔE_ν, the lifetimes extracted from the system (A19) at steady state. This self-consistent approach is handled by iterations. We store in look-up tables the variables $S_\nu(F)$, $T_\nu(F)$, and $G_\nu(F)$, together with the energies $\Delta E^*(F)$ and $\Delta E_\nu(F)$, and the scattering rates into the trap levels.

(ii) We distribute a random ensemble of Coulombic traps in the simulation volume (typically 10 nm$\times$10 nm$\times d_{\text{ox}}$, d_{ox} being the SiO_2 thickness) according to the experimentally determined density and depth distribution of the traps. After solving the Poisson equation for this ensemble of traps and with boundary conditions determined for the average field F, we determine the local field at each trap. We should stress that this local field F_{loc} is quite different from the experimentally measured F, as the *proximity of other Coulombic wells strongly distorts the environment of each trap.*

(iii) We use our "conventional" MC algorithm[24] to simulate electron transport in SiO_2 in the field obtained from the Poisson solution with the particular trap ensemble selected. The only additional process we include are the scattering into the pseudocontinuum at E^* and into the localized states of each trap. The rate at which electrons enter the levels E^* and E_ν provides a statistical evaluation of the supply functions Φ^* and Φ_ν in Eq. (A19). Once an electron enters the level E_ν, we consider it trapped, thermally reemitted, or field ionized according to the probabilities $S_\nu(F_{\text{loc}})$, $G_\nu(F_{\text{loc}})$, and $T_\nu(F_{\text{loc}})$, respectively, corresponding to the particular trap. We obtain these values from an interpolation using previously generated tables. Tunnel and thermally reemitted electrons are reintroduced into the simulation.

(iv) After a sufficient time, the simulation is halted and a trapping probability is obtained by dividing the number of trapped electrons by the total number of injected particles. Dividing this trapping probability by the areal trap density, we obtain the cross section for electron trapping *for this particular trap ensemble.*

(v) Finally, we repeat the procedure for different ensembles, as the small number of traps simulated introduces large statistical variations. An ensemble average of the capture cross section is taken at the end.

We conclude by noticing that, the simulation being quite CPU intensive, the "quantum Monte Carlo" data shown in Fig. 5 are affected by a large noise, the standard deviation being on the average twice the value of the cross section. Nevertheless, the order of magnitude and the qualitative behavior of the data in Fig. 5 are unlikely to be affected by the poor statistics.

APPENDIX B

To describe the model potential for neutral traps in SiO_2, we have followed Lax[36] and have employed the dipole potential

$$V(r)=\frac{1}{2}\frac{e\Pi}{4\pi\epsilon_{\text{ox}}r^2}\ , \qquad \text{(B1)}$$

where r is the distance from the center of the trap and Π is the dipole induced by an electron on a defect center of polarizability α:

$$\Pi=\alpha E=\alpha\frac{e}{4\pi\epsilon_{\text{ox}}r^2}\ , \qquad \text{(B2)}$$

where E is the magnitude of the (dipole) electric field. Lax gives a rough estimate of the polarizability α in terms of the polarizability α_H and ionization energy Ry_H of the hydrogen atom in vacuum:[36]

$$\alpha\simeq\alpha_\text{H}\frac{m_{\text{el}}}{m^*}\left[\frac{\text{Ry}_\text{H}}{\text{Ry}_{\text{ox}}}\right]^2\ , \qquad \text{(B3)}$$

where m_{el} is the free electron mass and m^* is the effective mass in the solid. For SiO_2, using $m^*=m_{\text{el}}$, and the value for α_H given in Ref. 36, we have

$$V(r)=-\frac{A}{r^4}\ , \qquad \text{(B4a)}$$

with

$$A=\frac{1}{2}\frac{\alpha e^2}{(4\pi\epsilon_{\text{ox}})^2}=41.5\ \text{eV}\,\text{Å}^4\ . \qquad \text{(B4b)}$$

[1]D. J. DiMaria, Appl. Phys. Lett. **51**, 665 (1987).
[2]D. J. DiMaria and J. Stasiak, J. Appl. Phys. **65**, 2342 (1989).
[3]P. Fazan, M. Dutoit, C. Martin, and M. Ilegems, Solid State Electron. **30**, 829 (1987).
[4]E. Avni and J. Shappir, Appl. Phys. Lett. **51**, 463 (1987).
[5]J. M. Sung and S. A. Lyon, Appl. Phys. Lett. **50**, 1152 (1987).
[6]I. C. Chen, S. Holland, and C. Hu, J. Appl. Phys. **61**, 4544 (1987).
[7]M. Aslam, J. Appl. Phys. **62**, 159 (1987).
[8]Y. Nissen-Cohen, J. Shappir, and D. Frohman-Bentchkowsky, J. Appl. Phys. **60**, 2024 (1986).
[9]M. M. Heyns, R. F. DeKeersmaecker, and M. W. Hillen, Appl. Phys. Lett. **44**, 202 (1984).
[10]M. M. Heyns, and R. F. DeKeersmaecker, J. Appl. Phys. **58**, 3936 (1984).
[11]Y. Nissen-Cohen and T. Gorczyca, Electron. Dev. Lett. **EDL-9**, 287 (1988).
[12]A. Badihi, E. Eitan, I. Cohen, and J. Shappir, Appl. Phys. Lett. **40**, 396 (1982).
[13]R. F. DeKeersmaecker and D. J. DiMaria, J. Appl. Phys. **51**, 1085 (1980).
[14]R. F. DeKeersmaecker and D. J. DiMaria, J. Appl. Phys. **51**, 532 (1980).
[15]D. A. Buchanan, M. V. Fischetti, and D. J. DiMaria, Appl. Surf. Sci. **39**, 420 (1989).
[16]S. K. Lai and D. R. Young, J. Appl. Phys. **52**, 6231 (1981).
[17]Y. Y. Kim and P. M. Lenahan, J. Appl. Phys. **64**, 3551 (1988).
[18]P. M. Lenahan and P. V. Dressendorfer, J. Appl. Phys. **55**, 3495 (1984).
[19]L. P. Trombetta, G. J. Gerardi, D. J. DiMaria, and E. Tierney, J. Appl. Phys. **64**, 2434 (1988).
[20]G. A. Scoggan and T. P. Ma, J. Appl. Phys. **48**, 294 (1977).
[21]D. J. DiMaria, in *The Physics of SiO_2 and its Interfaces,* edited by S. T. Pantelides (Pergamon, New York, 1978), pp. 160–178.
[22]R. C. Hughes, Phys. Rev. Lett. **35**, 449 (1975).
[23]T. H. Ning, J. Appl. Phys. **47**, 3203 (1976).
[24]M. V. Fischetti, D. J. DiMaria, S. D. Brorson, T. N. Theis, and J. R. Kirtley, Phys. Rev. B **31**, 8124 (1985).
[25]M. V. Fischetti and D. J. DiMaria, Phys. Rev. Lett. **55**, 2475 (1985).
[26]S. D. Brorson, D. J. DiMaria, M. V. Fischetti, F. L. Pesavento, P. M. Solomon, and D. W. Dong, J. Appl. Phys. **58**, 1302 (1985).
[27]D. J. DiMaria, M. V. Fischetti, E. Tierney, and S. D. Brorson, Phys. Rev. Lett. **56**, 1284 (1985).
[28]D. J. DiMaria, M. V. Fischetti, M. Arienzo, and E. Tierney, J. Appl. Phys. **60**, 1719 (1986).
[29]D. J. DiMaria, M. V. Fischetti, J. Batey, L. Dori, E. Tierney, and J. Stasiak, Phys. Rev. Lett. **57**, 3213 (1986).
[30]M. V. Fischetti, D. J. DiMaria, L. Dori, J. Batey, E. Tierney, and J. Stasiak, Phys. Rev. B **35**, 4404 (1987).
[31]J. M. Aitken and D. R. Young, J. Appl. Phys. **47**, 1196 (1976).
[32]D. J. DiMaria, J. Appl. Phys. **47**, 4073 (1976).
[33]L. Trombetta, R. J. Zeto, and F. J. Feigl, J. Appl. Phys. **62**, 1913 (1987).
[34]R. J. Powell and C. N. Berglund, J. Appl. Phys. **42**, 4390 (1976).
[35]M. Lax, J. Phys. Chem. Solids **8**, 66 (1959).
[36]M. Lax, Phys. Rev. **119**, 1502 (1960).
[37]G. A. Dussel and K. W. Böer, Phys. Status Solidi **39**, 375 (1970).
[38]Ning (Ref. 43) found that the Eqs. (7a) and (7b) in the paper of Dussel and Böer (Ref. 37) contained typographical errors. His expressions (3.3)–(3.7) were derived from Eqs. (5) and (6) in the paper of Dussel and Böer. Ning's corrected expressions agree well with those we calculated using numerical integration techniques and are assumed to be correct.
[39]J. D. Bekenstein and J. B. Krieger, Phys. Rev. **130**, 130 (1969).
[40]S. Chaudhum, D. D. Coon, G. E. Derkits, and J. R. Banavar, Phys. Rev. A **23**, 1657 (1971).
[41]A. Messiah, *Quantum Mechanics* (North-Holland, Amsterdam, 1970).
[42]J. M. Aitken, D. R. Young, and K. Pan, J. Appl. Phys. **49**, 3386 (1978).
[43]T. H. Ning, J. Appl. Phys. **49**, 4082 (1978).
[44]T. Yamabe, A. Akitomo, and H. J. Silverstone, Phys. Rev. A **16**, 887 (1977).